19

Computational fluid dynamics

Computational fluid dynamics (CFD) is a whole field in its own right [37, 38, 40]. Swift modern computers have to a large extent replaced wind tunnels and wave tanks for the design of airplanes, ships, cars, bridges, and in fact any human construction that is meant to operate in a fluid. The same richness of phenomena which makes analytic solutions to the equations of fluid mechanics difficult to obtain, also makes these equations hard to handle by direct numerical methods. Secondary flows, instabilities, vortices of all sizes, and turbulence complicate matters and may require numerical precision that can be hard to attain. The infinite speed of sound in incompressible fluids creates its own problems, and on top of that there are intrinsic approximation errors and instabilities.

As in numeric elastostatics (chapter 12) there is a number of steps that must be carried out in any simulation. First of all, it is necessary to clarify which equations one wishes to solve and already there make simplifications to the problem or class of problems at hand. Secondly, continuous space must be discretized, and here there is a variety of methods based on finite differences, finite elements, or finite volumes. Thirdly, a discrete dynamic process must be set up which guides the initial field configuration towards the desired solution. Most often this process emulates the time evolution of fluid dynamics itself, as described by the Navier-Stokes equations. Finally, convergence criteria and error estimates are needed to monitor and gain confidence in the numerical solutions.

The methods presented in this chapter are applicable to a variety of steady and unsteady flow problems. Here we shall only compute two-dimensional laminar flow in a channel of finite length between parallel plates and determine how it turns into the well-known parabolic Poiseuille profile downstream from the entrance, and how far the influence of the entrance reaches.

Copyright © 1998–2002, Benny Lautrup

19.1 Unsteady, incompressible flow

In numeric elastostatics (chapter 12) we were able to set up an artificial dissipative dynamics, called gradient descent, that guided the displacement field towards a static solution with minimal elastic energy. This technique cannot be transferred to computational fluid dynamics, because a solution to the steady-state equations does not correspond to an extremum of any bounded quantity (problem 19.1). Instead we shall attempt to copy Nature by simulating the complete set of time-dependent Navier-Stokes equations (17-12). Appealing to the behavior of real fluids, the natural viscous dissipation built into these equations should hopefully guide the velocity field towards a steady-state solution.

There is, however, no guarantee — neither from Nature nor from the equations — that the flow will always settle down and become steady, even when the boundary conditions are time-independent. We are all too familiar with the unsteady and sometimes turbulent flow that may spontaneously arise under even the steadiest of circumstances, as for example a slow river narrowing down or even worse, coming to a water fall. But this is actually not so bad, because a forced steady-state solution is completely uninteresting when the real fluid refuses to end up up in that state. We do, for example, not care much for the Poiseuille solution (18-21) to pipe flow at a Reynolds number beyond the transition to turbulence, or for that matter the laminar flow around a sphere in an ideal fluid (section 15.7). If steady flow is desired, one must keep the Reynolds number so low that there is a chance for it to become established.

Field equations

In order not to complicate matters we shall only consider incompressible fluids with constant density $\rho = \rho_0$, implying the vanishing of the divergence at all times,

$$\mathsf{div}\, \boldsymbol{v} = 0 \ . \tag{19-1}$$

The Navier-Stokes equation (17-12) is written as an equation of motion for the velocity field,

$$\frac{\partial \boldsymbol{v}}{\partial t} = \boldsymbol{F} - \boldsymbol{\nabla} \widetilde{p}, \tag{19-2}$$

with

$$\boldsymbol{F} = -(\boldsymbol{v} \cdot \boldsymbol{\nabla})\boldsymbol{v} + \nu \boldsymbol{\nabla}^2 \boldsymbol{v} + \boldsymbol{g} \ , \tag{19-3}$$

where $\nu = \eta/\rho_0$ is the kinematic viscosity, and $\widetilde{p} = p/\rho_0$ is the 'kinematic pressure'. For convenience we have also introduced a special symbol $\boldsymbol{F}$ to denote the local acceleration arising from inertia, viscosity and gravity, but not pressure. The gravitational field could in principle be included as an effective pressure (15-13), although that would obscure the boundary conditions we might want to impose on the real pressure. In the following we shall simply assume that the field of gravity is constant.

Copyright © 1998–2002, Benny Lautrup

Poisson equation for pressure

In incompressible flow the pressure is determined indirectly through the vanishing of the divergence of the velocity field. Calculating the divergence of both sides of (19-2), we find

$$\nabla^2 \widetilde{p} = \operatorname{div} \boldsymbol{F} \ . \tag{19-4}$$

This is the condition which must be fulfilled in order that the velocity field remains free of divergence at all times. Knowing the velocity field $\boldsymbol{v}$ at a given time we can calculate the right hand side and solve this equation with suitable boundary conditions to determine the pressure everywhere in the fluid at that particular instant of time.

Solutions to the Poisson equation are, however, non-local functions of the source, basically of the same form as the gravitational potential (3-27). Any local change in the velocity field at a point $\boldsymbol{x}'$ is via the Poisson equation above *instantaneously* communicated to the pressure at any other point $\boldsymbol{x}$ in the fluid, albeit damped by the $|\boldsymbol{x} - \boldsymbol{x}'|^{-1}$-dependence on distance. The non-local changes in pressure are then communicated back to the velocity field via the Navier-Stokes equation (19-2). The pressure thus links the velocity field at any instant of time non-locally to its immediately preceding values, even for infinitesimally small time intervals. Pressure informs the world at large about the present state of the incompressible velocity field faster than even gossip could!

Physically, the unpleasant non-local behavior can be traced back to the assumption of absolute incompressibility (19-1), which is just as untenable in the real world of local interactions as absolute rigidity. So, we have again come up against a physical limit arising from our simplifying assumptions. As pointed out before, incompressibility should be viewed as a property of the flow rather than of the fluid itself. The unavoidable compressibility of real matter will in fact limit the rate at which pressure changes can propagate through a fluid to the speed of sound. Nevertheless, such a conclusion does not detract from the practical usefulness of the divergence condition (19-1) for 'normal' flow speeds well below the speed of sound.

Boundary conditions

In many fluid dynamics problems, fixed impermeable walls guide the fluid between openings where it enters and leaves the system. On fixed walls the velocity field must vanish at all times, because of the impermeability and no-slip conditions which respectively require the normal and tangential components to vanish. Setting $\boldsymbol{v} = \boldsymbol{0}$ on the left hand side of the equation of motion (19-2) we obtain a boundary condition for pressure, $\nabla \widetilde{p} = \boldsymbol{F}$. The same is the case at a fluid inlet, where the velocity field is fixed to an externally defined constant value, $\boldsymbol{v} = \boldsymbol{v}_0$. Outlet velocities are usually not controlled externally, and as a boundary condition on the velocity field one may choose the vanishing of the normal derivative, $(\boldsymbol{n} \cdot \nabla)\boldsymbol{v} = \boldsymbol{0}$. Alternatively, the stress vector may be required to vanish, but that is harder to implement.

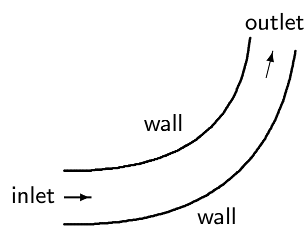

19.2 Temporal discretization

Suppose the current velocity field is $\boldsymbol{v}(\boldsymbol{x},t)$ and the current pressure field $\widetilde{p}(\boldsymbol{x},t)$. From these fields we may calculate the current acceleration field $\boldsymbol{F}(\boldsymbol{x},t)$ and then use the equation of motion (19-2) to move the velocity field forward in time through a small but finite time step Δt,

$$\boldsymbol{v}(\boldsymbol{x},t+\Delta t) = \boldsymbol{v}(\boldsymbol{x},t) + \big(\boldsymbol{F}(\boldsymbol{x},t) - \boldsymbol{\nabla}\widetilde{p}(\boldsymbol{x},t)\big)\Delta t \ . \tag{19-5}$$

Taylor expansion of the left hand side shows that the error is $\mathcal{O}\left(\Delta t^2\right)$, but less error-prone higher-order schemes are also possible [38, 37]. Provided the velocity field is free of divergence and the pressure satisfies (19-4), the new velocity field obtained from this equation will also be free of divergence.

Divergence suppression

But approximation errors cannot be avoided in any finite step algorithm. Since the current velocity field may not be perfectly free of divergence, it is more appropriate to demand that the new velocity field is free of divergence, *i.e.* $\mathsf{div}\,\boldsymbol{v}(\boldsymbol{x},t+\Delta t) = \boldsymbol{0}$. Calculating the divergence of both sides of (19-5) we obtain a modified Poisson equation for the pressure

$$\boldsymbol{\nabla}^2\widetilde{p} = \mathsf{div}\,\boldsymbol{F} + \frac{\mathsf{div}\,\boldsymbol{v}}{\Delta t} \ . \tag{19-6}$$

The factor $1/\Delta t$ amplifies the divergence errors, so that this Poisson equation will primarily be concerned with correction of divergence errors and only when they have been suppressed will the acceleration field $\boldsymbol{F}$ gain influence on the pressure. In practice, the stepping algorithm (19-5) can get into trouble if the divergence becomes too large. It is for this reason important to secure that the initial velocity field is reasonably free of divergence, but in a complicated flow geometry that can in fact be quite hard to attain.

Stability conditions

There are essentially only two possibilities for what can happen to the approximation errors in the course of many time steps. Either the errors will become systematically larger, in which case the computation goes straight to the land of meaningless results, or the errors will diminish or at least stay constant and ‘small’, thereby keeping the computation on track. It takes careful mathematical analysis to determine a precise value for the upper limit to the size of the time step. The result depends strongly on both the spatial and temporal discretization (see for example [38, 34]), and may range from zero to infinity depending on the particular algorithm that is implemented.

Here we shall present an intuitive argument for the stability conditions that apply to the straight-forward numerical simulation (19-5) on a spatial grid with

Copyright © 1998–2002, Benny Lautrup

typical coordinate spacings Δx, Δy, and Δz. These conditions may be understood from the physical processes that compete in displacing fluid particles in, say, the x-direction. One is momentum diffusion due to viscosity which effectively displaces the particle by $\sqrt{\nu \Delta t}$ in a time interval Δt (see page 289). Another is advection with velocity v_x which displaces the particle a distance $|v_x|\,\Delta t$. Finally, there is the gravitational field which typically displaces the particle by $g_x \Delta t^2$. Intuitively, it seems reasonable to demand that all these displacements be smaller than the grid spacing,

$$\sqrt{\nu \Delta t} \lesssim \Delta x \ , \quad |v_x|\,\Delta t \lesssim \Delta x \ , \quad g_x \Delta t^2 \lesssim \Delta x \tag{19-7}$$

Taking into account that the maximal velocity provides the most stringent advective condition, the global condition may be taken to be

$$\Delta t \lesssim \min\left(\frac{\Delta x^2}{\nu}, \frac{\Delta x}{|v_x|_{\max}}, \sqrt{\frac{\Delta x}{g_x}}\right) \ , \tag{19-8}$$

and similarly for the other coordinate directions. In practice trial-and-error may be used to determine where in the neighborhood of the smallest of these limits instability actually sets in.

The diffusive condition is most restrictive for large viscosity, the advective for high velocities, and the gravitational in strong gravity. The allowed time step is generally largest for the coarsest spatial grid, which on the other hand is blind to finer details of the flow. Thus there is a payoff between the detail desired in the simulation and its rate of progress. High detail entails slow progress, and thus a high cost in computer time.

19.3 Spatial discretization

In the discussion of numeric elastostatics we described a method based on finite differences with errors of only second order in the grid spacings (section 12.2 on page 195). Although it is possible to solve simple flow problems using this method, most such problems will benefit from a somewhat more sophisticated treatment. The method of *staggered grids* to be presented here comes at essentially no cost in computer memory or time, but does complicate matters a bit. A number of applications of this method are given in [37].

Restriction to two dimensions

For simplicity we shall limit the following discussion to two-dimensional flow in the xy-plane, as exemplified by the flow in a channel between parallel plates (section 18.2 on page 303). The restriction to two dimensions still leaves ample room for interesting applications. Generalization to three dimensions is straightforward.

Copyright © 1998–2002, Benny Lautrup

Two-dimensionality is taken to mean that the fields can only depend on x and y and that $v_z = 0$. The equations of motion now simplify to

$$\frac{\partial v_x}{\partial t} = F_x - \nabla_x \widetilde{p} \ , \qquad \frac{\partial v_y}{\partial t} = F_y - \nabla_y \widetilde{p} \ , \tag{19-9}$$

with

$$F_x = -v_x \nabla_x v_x - v_y \nabla_y v_x + \nu \left(\nabla_x^2 + \nabla_y^2\right) v_x + g_x \ , \tag{19-10a}$$

$$F_y = -v_x \nabla_x v_y - v_y \nabla_y v_y + \nu \left(\nabla_x^2 + \nabla_y^2\right) v_y + g_y \ , \tag{19-10b}$$

and the divergence condition becomes

$$\nabla_x v_x + \nabla_y v_y = 0 \ . \tag{19-11}$$

The stresses may of course be calculated, but are not as important here as in numeric elastostatics, because boundary conditions most often are specified directly in terms of the velocities.

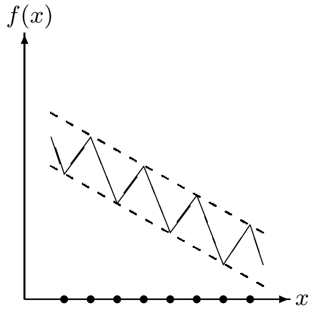

The fully drawn zigzag-curve $f(x)$ between the two straight lines has constant central difference (12-4) on the grid! Such zigzag behavior is typical of the 'leapfrog' errors that may arise when using the naive central differencing scheme of section 12.2.

Midpoint differences

The main objection to the central difference $\widehat{\nabla}_x f(x)$ defined in (12-4) is that it spans twice the fixed interval Δx around the central point x to which it 'belongs'. As was remarked there, this opens for 'leapfrog' or 'flipflop' instabilities in which neighboring grid points behave quite differently. The problem becomes particularly acute in the interplay between the equations of motion and the instantaneous Poisson equation for pressure.

One way out is to recognize that the difference in field values between two neighboring grid-points properly 'belongs' to the midpoint of the line that connects them. If we denote the coordinates of the points by $x \pm \frac{1}{2}\Delta x$ the central difference around the midpoint x,

$$\widehat{\nabla}_x f(x) = \frac{f\left(x + \frac{1}{2}\Delta x\right) - f\left(x - \frac{1}{2}\Delta x\right)}{\Delta x} \ , \tag{19-12}$$

has errors of only second order in the grid spacing. This is what is really meant by saying that the difference 'belongs' to the midpoint.

But the midpoints between grid points are not themselves part of the grid. We could of course double the grid and use $\frac{1}{2}\Delta x$ as grid-spacing, thereby including the midpoints, but that would just bring us back to the situation we started out to correct. Instead we shall think of the midpoint values of fields and their derivatives as being *virtual*, meaning that they may arise during a calculation but are not retained as part of the information kept about the fields on the grid.

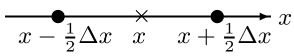

The finite difference between the grid points $x \pm \frac{1}{2}\Delta x$ belongs to the point x.

Staggered grids

To see how this works out, let us discretize the divergence condition (19-11) writing it in terms of midpoint differences in the point (x, y)

$$\widehat{\nabla}_x v_x(x,y) + \widehat{\nabla}_y v_y(x,y) = 0 \ . \tag{19-13}$$

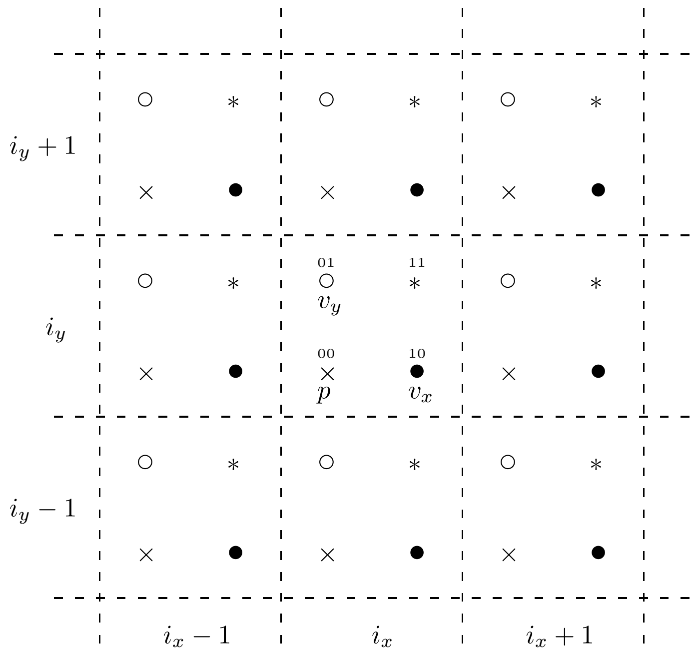

Figure 19.1: *Staggered grids. Four rectangular grids with uniform coordinate spacings Δx and Δy are shifted with respect to each other by half intervals. Three of the grids are naturally associated with the fundamental fields: the 00-grid (crosses) carries p, the 01-grid (full circles) carries v_x, and the 10-grid (open circles) carries v_y. The 11-grid (asterisks) carries only derivatives of the fundamental fields. The whole grid may be viewed as as a tiling of the plane with congruent cells of size $\Delta x \times \Delta y$, numbered by integers i_x and i_y, as shown.*

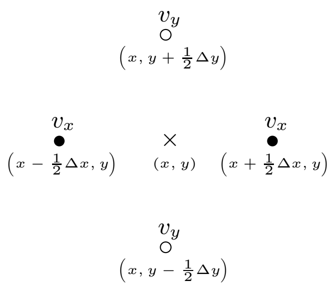

The grid for v_x (full circles) and the grid for v_y (open circles) do not overlap but have common midpoints (crosses) in which the divergence condition can be imposed.

Since (x, y) has to be the common midpoint for both coordinate directions, we should have direct access to v_x in $\left(x \pm \frac{1}{2}\Delta x, y\right)$ and v_y in $\left(x, y \pm \frac{1}{2}\Delta y\right)$, but not necessarily in (x, y). Repeating this argument throughout space (see fig. 19.1), we conclude that the grids for the fields v_x and v_y do not overlap anywhere, but are systematically shifted, or *staggered*, with respect to each other.

In effect we *have* doubled the grid in both spatial directions, but the new grid is viewed as composed of four interlaced grids of the original type, each carrying some of the fields and their derivatives. Systematically, the coordinates of the four grids may be written

$$x = x_0 + i_x \Delta x + j_x \frac{1}{2} \Delta x \tag{19-14a}$$

$$y = y_0 + i_y \Delta y + j_y \frac{1}{2} \Delta y \tag{19-14b}$$

where i_x, i_y are integers and j_x, j_y are binary, taking only the values 0 or 1. The grid of common midpoints used in calculating the divergence is arbitrarily chosen to be $j_x = j_y = 0$, so that we may denote the four grids by 00, 10, 01, and 11 (marked with different symbols in fig. 19.1). Thus, v_x is defined on the 10-grid and v_y on the 01-grid. We shall see below that the pressure p naturally belongs to the 00-grid, whereas there is no fundamental field associated with the 11-grid, but only derivatives of the fields (see however problem 19.3).

Copyright © 1998–2002, Benny Lautrup

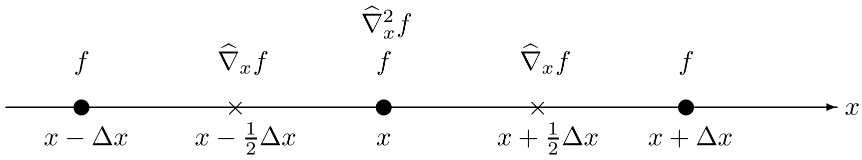

Figure 19.2: *A double derivative is represented by the midpoint difference of the two neighboring single derivatives, themselves represented by midpoint differences. Conveniently, it ends up on the same grid as the field itself.*

The four staggered grids create a *tiling* of the plane with rectangular cells numbered by i_x and i_y, each cell containing four grid points numbered by j_x and j_y. Generalization of this scheme to three dimensions is straightforward, though harder to visualize. In three dimensions there will be eight staggered grids characterized by three integers and three binary variables.

Double differences

A double derivative, say ∇_x^2, is particularly simple when represented by midpoint differences. Combining the two levels of midpoint differencing we obtain (see fig. 19.2)

$$\widehat{\nabla}_x^2 f(x) = \frac{f(x+\Delta x) + f(x-\Delta x) - 2f(x)}{\Delta x^2} , \tag{19-15}$$

and because of the symmetry in Δx the errors are of second order only. Geometrically the two levels of midpoint differences bring the double derivative back to the point it 'originated in', so that both $\widehat{\nabla}_x^2 v_x$ and $\widehat{\nabla}_y^2 v_x$ belong to the same grid as v_x (*i.e.* 10).

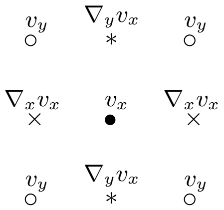

The differences $\widehat{\nabla}_x v_x$ and $\widehat{\nabla}_y v_x$ in a 10-point (filled circle) may be found as averages of the neighboring values on the 00 and 11-grids, respectively marked by crosses and asterisks. The value of v_y on the 10-grid is obtained by averaging over all four nearest neighbors on the 01-grid (open circle).

Discretized equations of motion

The local acceleration fields F_x and F_y should be discretized on the same grids as v_x and v_y (*i.e.* on 10 and 01) for the equations of motion (19-9) to be fulfilled with fields and derivatives calculated in the same point.

The double derivatives in the viscous terms present in this respect no problems, and neither does the gravitational acceleration nor the pressure gradient which automatically ends up on the right grids. In the inertial term, $-v_x \nabla_x v_x$, there is the problem that $\widehat{\nabla}_x v_x$ belongs to the 00-grid and not to the 10-grid as we would like it to. In order to keep errors to second order one must form the average of $\widehat{\nabla}_x v_x$ over the two neighboring 00-values. Similarly, in the inertial term, $-v_y \nabla_y v_x$, the derivative $\widehat{\nabla}_y v_x$ is naturally found on the 11-grid, it must also be averaged over the two nearest neighbors to get its 10-value. The worst case is v_y for which the value on the 10-grid is obtained as the average over the four nearest neighbors on the 01-grid.

Copyright © 1998–2002, Benny Lautrup

Marking the averaged quantities with brackets we may write the discretized acceleration fields in the form (see problem 19.4 for the explicit expressions)

$$F_x = -v_x \left\langle \widehat{\nabla}_x v_x \right\rangle - \langle v_y \rangle \left\langle \widehat{\nabla}_y v_x \right\rangle + \nu \left(\widehat{\nabla}_x^2 + \widehat{\nabla}_y^2 \right) v_x + g_x \ , \qquad \text{(19-16a)}$$

$$F_y = - \langle v_x \rangle \left\langle \widehat{\nabla}_x v_y \right\rangle - v_y \left\langle \widehat{\nabla}_y v_y \right\rangle + \nu \left(\widehat{\nabla}_x^2 + \widehat{\nabla}_y^2 \right) v_y + g_y \ . \qquad \text{(19-16b)}$$

It must be remarked that there is more than one way of calculating the inertial terms, even if errors are required to be of second order only.

Finally, the discretized equations of motion (19-5) become

$$v_x(x, y, t + \Delta t) = v_x(x, y, t) + \big(F_x(x, y, t) - \widehat{\nabla}_x \widetilde{p}(x, y, t)\big)\Delta t \ , \qquad \text{(19-17a)}$$

$$v_y(x, y, t + \Delta t) = v_y(x, y, t) + \big(F_y(x, y, t) - \widehat{\nabla}_y \widetilde{p}(x, y, t)\big)\Delta t \ , \qquad \text{(19-17b)}$$

to be evaluated on the 10 and 01-grids, respectively.

Solving the discrete Poisson equation

During an iteration cycle the accelerations (19-16) are calculated from the current values of the discrete fields at time t, and afterwards the corresponding pressure at time t is calculated by solving the discretized version of the Poisson equation (19-6),

$$\left(\widehat{\nabla}_x^2 + \widehat{\nabla}_y^2 \right) \widetilde{p} = \widehat{\nabla}_x F_x + \widehat{\nabla}_y F_y + \frac{\widehat{\nabla}_x v_x + \widehat{\nabla}_y v_y}{\Delta t} \ . \qquad \text{(19-18)}$$

The solution to this equation may be found by means of relaxation methods, for example gradient descent (see section 12.1 on page 194), in which the pressure $\widetilde{p}(x, y, t)$ undergoes successive changes of the form

$$\delta \widetilde{p} = \epsilon \left(\left(\widehat{\nabla}_x^2 + \widehat{\nabla}_y^2 \right) \widetilde{p} - s \right) \ , \qquad \text{(19-19)}$$

where $\epsilon > 0$ the step size and $s(x, y, t)$ is the source (the right hand side of (19-18)). The relaxation algorithm converges towards a solution to $\boldsymbol{\nabla}^2 \widetilde{p} = s$ for sufficiently small ϵ because it descends along the steepest downwards gradient towards the unique minimum of a quadratic ‘energy’-function (see problem 19.2).

Denoting the n'th approximation to the solution by $\widetilde{p}_n(x, y, t)$ and replacing the derivatives by differences, the discretized relaxation process may be written explicitly as

$$\widetilde{p}_{n+1}(x, y, t) = \widetilde{p}_n(x, y, t) + \epsilon \left(\left(\widehat{\nabla}_x^2 + \widehat{\nabla}_y^2 \right) \widetilde{p}_n(x, y, t) - s(x, y, t) \right) \ . \qquad \text{(19-20)}$$

Starting with some field configuration $\widetilde{p}_0(x, y, t)$ and imposing boundary conditions after each step, this process will eventually lead to the desired solution, $\widetilde{p}(x, y, t)$. The problem is, however, that simple gradient descent is slow, too slow in fact to be applied inside every time step. *Conjugate gradient descent* [34, p.

Copyright © 1998–2002, Benny Lautrup

420] offers considerable speed-up by calculating the optimal step-size directly, but as it turns out there are still faster methods.

From the double difference operator (19-15) we see that the coefficient of $\widetilde{p}_n$ in (19-20) is $1 - 2\epsilon(1/\Delta x^2 + 1/\Delta y^2)$, and this suggests the following reparametrization of the step-size

$$\epsilon = \frac{\omega}{2}\left(\frac{1}{\Delta x^2} + \frac{1}{\Delta y^2}\right)^{-1} , \tag{19-21}$$

where ω is the dimensionless *convergence parameter*. This choice allows a precise definition of what is meant by *underrelaxation* ($\omega < 1$) and *overrelaxation* ($\omega > 1$). Straightforward gradient descent, in which the new field ($\widetilde{p}_{n+1}$) is calculated all over the grid before replacing the old ($\widetilde{p}_n$), only converges when underrelaxed.

In *successive overrelaxation* or SOR (see [38, p. 231] and [37, p. 35]), the new value $\widetilde{p}_{n+1}(x, y, t)$ in a grid point replaces the old value $\widetilde{p}_n(x, y, t)$ as soon as it is calculated during a sweep of the grid. The method converges for $1 < \omega < 2$ and in practice the best value for ω may be located by trial-and-error, usually not far below the upper limit, say $\omega = 1.7 - 1.9$. Since this algorithm sweeps sequentially through the grid, one should be aware that it may create small asymmetry errors in an otherwise symmetric situation. But fast it is, on small grids often converging in just a few iterations, after an initial phase has passed.

19.4 Channel entrance flow

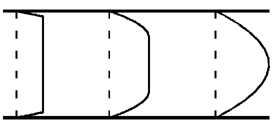

Sketch of the expected shape of the velocity profile at various distances downstream from the entrance.

A simple and — from the look of it — well-behaved problem concerns the steady flow pattern in a pipe or channel of width d in the vicinity of the entrance. Directly at the entrance, the flow is thought to be uniform with a flat velocity distribution which downstream smoothly turns into the characteristic parabolic Poiseuille shape. The typical distance for this to happen is the so-called *entrance length*, L'.

Momentum diffusion due to viscosity (page 289) tends to iron out all velocity gradients unless they are maintained by external forces. Near the entrance to the channel where the fluid speed is uniformly U, the velocity gradients and stresses on the sides are very large but soften progressively as the fluid moves downstream. The action of viscosity slows the fluid down near the sides of the channel, and since the volume flux must be the same everywhere in the channel, it has to speed up in the center.

Estimates

We have previously seen (page 289) that the diffusive momentum spread in a time interval t has a typical (90%) range of $\delta \approx 3\sqrt{\nu t}$ and reaches the middle of the channel from both sides for $3\sqrt{\nu t} \approx d/2$, or $t \approx 0.03\, d^2/\nu$. Multiplying with the velocity U we obtain an estimate for the entrance length, $L' \approx 0.03\, U d^2/\nu$,

Copyright © 1998–2002, Benny Lautrup

and introducing the Reynolds number $\mathsf{Re} = Ud/\nu$, we get

$$\frac{L'}{d} \approx k\ \mathsf{Re}\ , \tag{19-22}$$

with $k \approx 0.03$. For $\mathsf{Re} \approx 100$ which is squarely in the laminar region, the entrance length is thus estimated to be about 3 times the channel width, and about 60 times for $\mathsf{Re} \approx 2000$. In the turbulent regime the entrance length on the contrary decreases with growing Reynolds number (as $\mathsf{Re}^{-1/4}$) [?]. The influence of the entrance is always expected to be noticeable at least for a length of the same size as the channel width d. For smaller values of the Reynolds number, say for $k\mathsf{Re} \lesssim 1$, we consequently expect that L'/d becomes a fixed constant, independent of the Reynolds number.

In the present numerical simulation we shall attempt to verify the linear growth with Reynolds number in the laminar regime and determine the magnitude of the coefficient k as well as the constant value of L'/d for $k\,\mathsf{Re} \lesssim 1$.

Boundary conditions

For simplicity we shall only consider a channel between parallel plates, so that we may apply the two-dimensional formalism of the preceding section. At the western entrance to the channel, $x = 0$, the velocity field is uniform $v_x = U$ with no cross flow, $v_y = 0$. The exit flow at $x = L$ is determined by the dynamics, and we shall just assume that the flow has stabilized in this region with longitudinally constant velocities, $\nabla_x v_x = \nabla_x v_y = 0$, as in ideal Poiseuille flow. On the impermeable southern and northern walls of the channel we must of course have $v_y = 0$, together with the no-slip condition, $v_x = 0$. In velocity-driven flow, the boundary conditions on pressure follow from the velocity conditions, and will be discussed below.

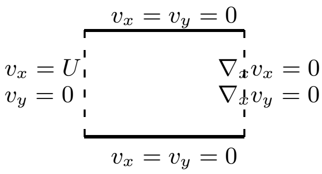

Boundary conditions for channel flow.

Initial data

The equations of motion must be supplied with initial data that fulfill the spatial boundary conditions and the condition of vanishing divergence. This is not nearly as simple as it sounds, even if there is great freedom in the choice of initial data and even if the final steady state is supposed to be independent of this choice. The problem becomes particularly acute if the boundaries are of irregular shape which they will always be in any realistic fluid flow problem.

Here we shall choose the initial velocity and pressure fields (at $t = 0$) to be

$$v_x = U\ , \quad v_y = 0\ , \quad \widetilde{p} = 0 \tag{19-23}$$

everywhere inside the channel. This certainly fulfills the divergence condition, but has a discontinuous jump on the sides of the channel due to the no-slip boundary conditions. The initial fields also fulfill the Poisson equation for pressure (19-6).

Copyright © 1998–2002, Benny Lautrup

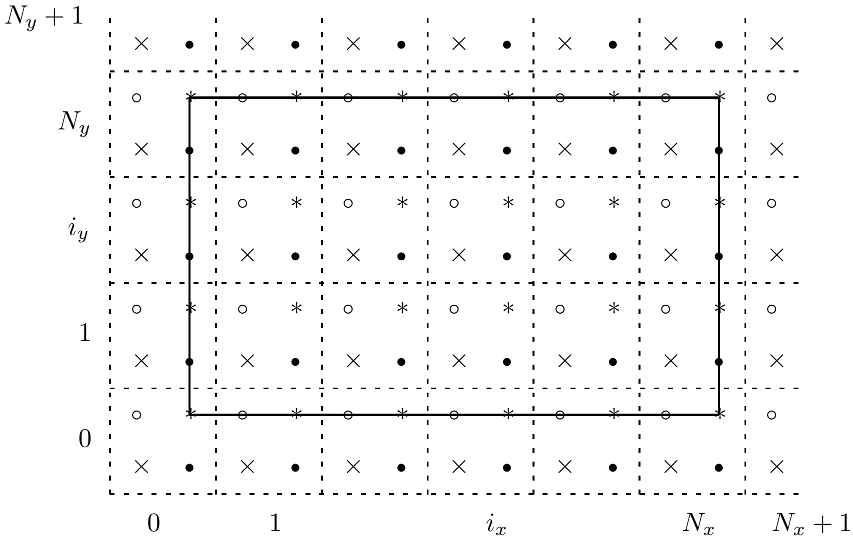

Figure 19.3: *A rectangular region (fully drawn) is discretized using staggered grids, here with $N_x = 5$ and $N_y = 3$. Boundary conditions necessitate one layer of data outside the region on all sides, requiring 7×5 basic cells. The velocity v_x is defined on the 10-points (filled circles), v_y on the 01-points (open circles) and the pressure $\widetilde{p}$ on the 00-points (crosses).*

The grid

The rectangular region of size $L \times d$ is discretized using staggered grids with coordinate intervals $\Delta x = L/N_x$ and $\Delta y = d/N_y$, where N_x and N_y are integers. This requires an array of $(N_x + 2) \times (N_y + 2)$ basic cells to cover the region of interest. In a computer program, any field value belonging to a basic cell is represented by an array, $f(x, y) \leftrightarrow f[i_x, i_y]$, indexed by the cell indices. At the 'eastern' and 'northern' borders only half the cell data is needed, as indicated in fig. 19.3.

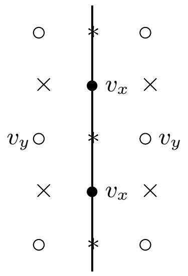

On the western boundary the value of the velocity v_x may be implemented directly, whereas the boundary value of the velocity v_y is calculated as an average over the two nearest neighbors on both sides.

The discrete boundary conditions have to reflect that not all field values are known precisely on the border. At the entrance, the v_x-condition remains $v_x = U$ because this field is known on the border, but the v_y-condition must be implemented as $\langle v_y \rangle = 0$, where the average is over the nearest points on both sides of the border. On the northern and southern walls, the roles are reversed, and we have $\langle v_x \rangle = 0$ and $v_y = 0$. At the eastern exit, the condition $\nabla_x v_y = 0$ become $\widehat{\nabla}_x v_y = 0$. Since there is no data on v_x east of the border, the condition $\widehat{\nabla}_x v_x = 0$ can only be approximatively implemented as a backwards difference, $\widehat{\nabla}_x^- v_x = 0$.

General theory of the Poisson equation [?] tells us that we either need to know the pressure itself or its normal derivative on the boundary. Since at all times $v_x = U$ on the western border, the time-step equation (19-17) implies that $\widehat{\nabla}_x \widetilde{p} = F_x$. The value of F_x on the western boundary (obtained from (19-16)) requires knowledge of v_x further to the west, data that is not available on the grid. As it turns out, we do in fact not need to know F_x on the border. To see

Copyright © 1998–2002, Benny Lautrup

this, the discretized Poisson equation (19-18) is written as

$$\widehat{\nabla}_x \left(\widehat{\nabla}_x \widetilde{p} - F_x\right) + \widehat{\nabla}_y \left(\widehat{\nabla}_y \widetilde{p} - F_y\right) = \frac{\widehat{\nabla}_x v_x + \widehat{\nabla}_y v_y}{\Delta t} \ . \tag{19-24}$$

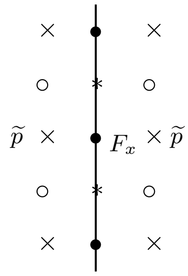

On the western boundary the normal difference of the pressure $\widehat{\nabla}_x \widetilde{p}$ is determined by F_x.

Since $\widehat{\nabla}_x \widetilde{p} = F_x$ on the border, the boundary value of $\widehat{\nabla}_x \widetilde{p} - F_x$ is always zero wherever it appears in the first term, independently of the boundary value of F_x. Thus, the value of F_x at the fluid inlet never appears in the Poisson equation and has therefore no influence on the solution. In practice, it is convenient to choose the boundary value $F_x = 0$, and correspondingly $\widehat{\nabla}_x \widetilde{p} = 0$.

On the solid walls $y = 0, d$, similar arguments lead to $\widehat{\nabla}_y \widetilde{p} = 0$. Finally, at $x = L$ we only know that $\widehat{\nabla}_x v_x = 0$ and consequently $\widehat{\nabla}_x^2 \widetilde{p} = \widehat{\nabla}_x F_x$ from the equation of motion (19-17). Again it follows from analysis of the Poisson equation that the actual boundary value of F_x cannot influence the solution. In this case one may either choose the pressure to be constant, $\langle \widetilde{p} \rangle = 0$, or better require $F_x = 0$ and $\widehat{\nabla}_x \widetilde{p} = 0$ at the exit.

Summarizing, the discrete boundary conditions are taken to be

$$v_x = U \ , \qquad \langle v_y \rangle = 0 \ , \qquad \widehat{\nabla}_x \widetilde{p} = 0 \ , \qquad \text{for } x = 0 \ , \tag{19-25a}$$

$$\widehat{\nabla}_x v_x = 0 \ , \qquad \widehat{\nabla}_x v_y = 0 \ , \qquad \widehat{\nabla}_x \widetilde{p} = 0 \ , \qquad \text{for } x = L \ , \tag{19-25b}$$

$$\langle v_x \rangle = 0 \ , \qquad v_y = 0 \ , \qquad \widehat{\nabla}_y \widetilde{p} = 0 \ , \qquad \text{for } y = 0, d \ . \tag{19-25c}$$

In the second line the difference $\widehat{\nabla}_x v_x$ actually belongs to the points inside the channel with $x = L - \Delta x/2$.

Monitoring the process

The most important quantity to monitor is the divergence which ideally should vanish. A convenient parameter is

$$\chi = \sqrt{\frac{\sum(\widehat{\nabla}_x v_x + \widehat{\nabla}_y v_y)^2}{\sum(\widehat{\nabla}_x v_x)^2 + (\widehat{\nabla}_y v_y)^2}} \tag{19-26}$$

where the sum runs over all internal grid points. It is dimensionless, independent of the grid for $N_x, N_y \to \infty$, and measures how well the two differences cancel each other in the divergence.

The convergence of the Poisson relaxation process (19-20) may be monitored by a similar parameter

$$\chi' = \Delta t \sqrt{\frac{\sum((\widehat{\nabla}_x^2 + \widehat{\nabla}_y^2)\widetilde{p} - s)^2}{\sum(\widehat{\nabla}_x v_x)^2 + (\widehat{\nabla}_y v_y)^2}} \ , \tag{19-27}$$

because this quantity is a dimensionless estimate of the average of the future divergence, $\mathsf{div}\, \boldsymbol{v}(t + \Delta t) = -(\boldsymbol{\nabla}^2 \widetilde{p} - s)\Delta t$.

Copyright © 1998–2002, Benny Lautrup

Iteration cycle

The grid arrays for all the fields, $v_x[i_x, i_y]$, $v_y[i_x, i_y]$, $\widetilde{p}[i_x, i_y]$, $F_x[i_x, i_y]$, and $F_y[i_x, i_y]$ are first cleared to zero, and then the velocity is initialized to $v_x[i_x, i_y] = U$ for $i_x = 0, \ldots, N_x$ and $i_y = 1, \ldots, N_y$.

Assuming that we have obtained a current set of discrete fields at time t, the following iteration cycle produces a new set of fields at $t + \Delta t$:

1. Calculate the new velocities v_x and v_y at time $t + \Delta t$ from (19-17) in all internal points (*i.e.* not on the boundary). Explicitly the internal grid points are given by $i_x = 1, \ldots, N_x - 1$ and $i_y = 1, \ldots, N_y$ for v_x, and $i_x = 1, \ldots, N_x$ and $i_y = 1, \ldots, N_y - 1$ for v_y.

2. Use the boundary conditions (19-25) to determine boundary values of the velocities. Explicitly they become

$$\begin{array}{lll} v_x[0, i_y] = U \ , & v_x[N_x, i_y] = v_x[N_x - 1, i_y] \ , & i_y = 1, \ldots, N_y \\ v_y[0, i_y] = -v_y[1, i_y] \ , & v_y[N_x + 1, i_y] = v_y[N_x, i_y] \ , & i_y = 1, \ldots, N_y - 1 \\ v_x[i_x, 0] = -v_x[i_x, 1] \ , & v_x[i_x, N_y + 1] = -v_x[i_x, N_y] \ , & i_x = 0, \ldots, N_x \\ v_y[i_x, 0] = 0 \ , & v_y[i_x, N_y] = 0 \ , & i_x = 0, \ldots, N_x + 1 \end{array}$$

   Notice the care that is necessary in the specifications of index ranges.

3. Calculate the new acceleration fields, F_x and F_y, in all internal points (with the same index ranges as for the velocities) from (19-16) using the new velocity fields. The boundary values of the accelerations remain zero.

4. Calculate the source of the Poisson equation (19-18) from the new fields in all internal points.

5. Solve the Poisson equation iteratively by means of the following subcycle

   (a) Apply the boundary conditions to the pressure. Explicitly they are

$$\begin{array}{lll} \widetilde{p}[0, i_y] = \widetilde{p}[1, i_y] \ , & \widetilde{p}[N_x + 1, i_y] = \widetilde{p}[N_x, i_y] \ , & i_y = 1, \ldots, N_y \\ \widetilde{p}[i_x, 0] = \widetilde{p}[i_x, 1] \ , & \widetilde{p}[i_x, N_y + 1] = \widetilde{p}[i_x, N_y] \ , & i_x = 0, \ldots, N_x + 1 \end{array}$$

   (b) Calculate the new pressure in all internal points using successive over-relaxation (SOR).

   (c) Repeat until the desired precision (χ') or the iteration limit are reached.

6. Repeat until the required time or iteration limits are reached.

At chosen intervals the grid arrays may be displayed graphically or written out to a file for later treatment.

Copyright © 1998–2002, Benny Lautrup

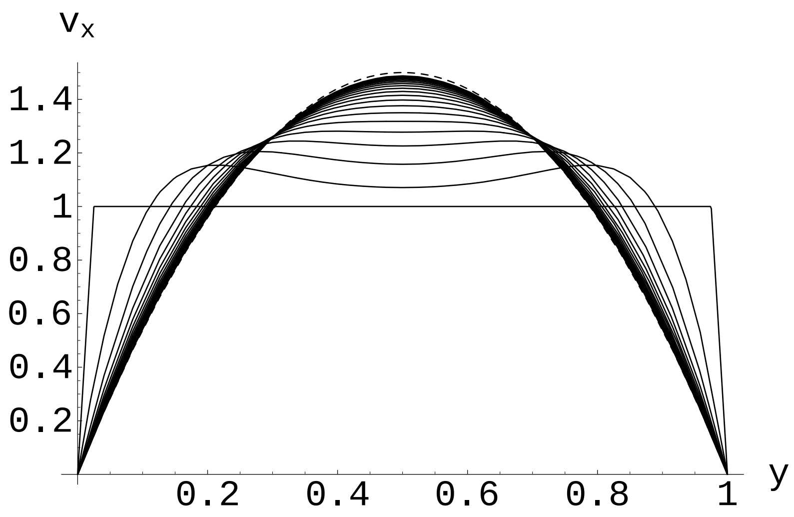

Figure 19.4: *Transformation of the steady velocity profile from the initial square shape to the parabolic Poiseuille shape (dashed) downstream from the entrance. The Reynolds number is chosen to be* $\mathsf{Re} = 100$*, the channel length* $L = 10$ *and width* $d = 1$*, and the curves are separated by* $\Delta x = 1/N_x$ *(with* $N_x = 40$*) in the interval* $0 \le x \le L/2$*.*

Results

We shall fix the mass scale by choosing unit density $\rho_0 = 1$, the length scale by choosing unit plate distance $d = 1$, and the time scale by setting the entry velocity $U = 1$. With these units the only parameter left in the problem are the (now dimensionless) kinematic viscosity ν and the (also dimensionless) length L of the channel. The Reynolds number is, for example, nothing but the reciprocal viscosity, $\mathsf{Re} = 1/\nu$. Here we shall mainly present results for $\mathsf{Re} = 100$. In view of the estimate (19-22) which predicts the entrance length to be 3 in this case, we choose $L = 10$. For $\mathsf{Re} \gtrsim 20$ the length is chosen to be $L = \mathsf{Re}/10$ whereas for $\mathsf{Re} \lesssim 20$ it is chosen to be $L = 2$, because the entrance length is expected to be constant. The grid dimensions are everywhere chosen to be $N_x = N_y = 40$.

In fig. 19.5 (left) the time evolution of the exit velocity is plotted together with the rise of the velocity in the channel. Allowing for maximally 100 SOR iterations, the process converges to $\chi' = 1\%$ in about 50 time steps, corresponding to $t = 0.3$. It reaches 95% of the Poiseuille maximal velocity $1.5U$ in 400 time steps corresponding to $t = 2.48$. The same is the case for the downstream rise of the velocity (fig. 19.5 right) which reaches 95% of its maximum at $x = 2.34$. The downstream evolution of the velocity profile towards the parabolic Poiseuille shape is shown in fig. 19.4. In fig. 19.6 (left) the pressure in the middle of the channel is plotted as a function of x, and it also reaches the Poiseuille form with constant gradient for $x \approx 2.5$.

Finally, in fig. 19.6 (right) the entrance length, defined as the point where v_x has reached 95% of maximum, has been plotted as a function of Reynolds number. It is remarkable that the same program with the identical convergence parameters covers a range of Reynolds numbers from nearly 0 to 5000. Below

Copyright © 1998–2002, Benny Lautrup

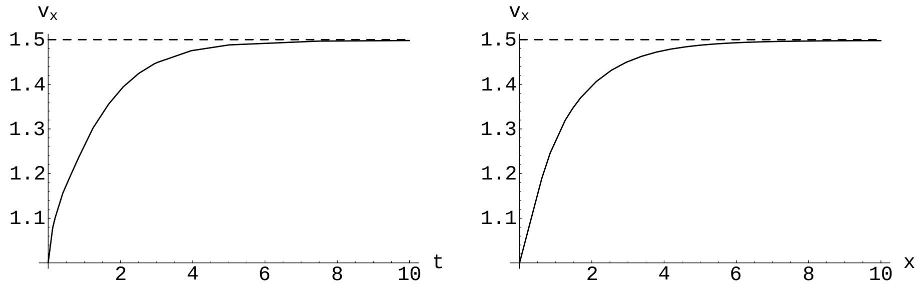

Figure 19.5: *The graph on the left shows the rise of the exit velocity $v_x(L, d/2, t)$ as a function of time, whereas the graph on the right shows the steady state velocity along the middle of the channel $v_x(x, d/2)$ as a function of x. The Reynolds number is 100. Both curves approach the Poiseuille maximal velocity of 1.5 times the average velocity.*

$\mathsf{Re} = 1$ the entrance length becomes constant, $L' = 0.43d$, and this makes sense because the influence of the entrance must always be noticeable at a distance compared to the channel width. At high Reynolds numbers ($\mathsf{Re} \gtrsim 200$) the linearity of the estimate (19-22) is confirmed and we obtain $k = 0.0197$ in good agreement with the rough estimate. There seems to be no sign of turbulence for Reynolds number between 2000 and 5000, but that could be due to the boundary conditions that impose too much smoothness of the velocity fields at the exit.

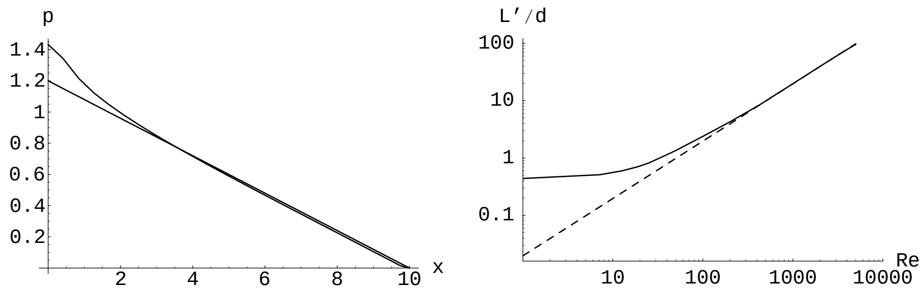

Figure 19.6: *The pressure is shown on the left as a function of distance x from the entrance. Its gradient becomes constant at about $x = 2.5$. The (95%) entrance length is plotted as a function of Reynolds number on the right. The dashed line corresponds to $L'/d = k\,\mathsf{Re}$ with $k = 0.0197$. For $\mathsf{Re} \lesssim 10$ the curve approaches the constant value 0.43.*

Problems

∗ **19.1** Show that it is not possible to find an integrated quantity F for which the equation for incompressible steady flow (18-4) corresponds to an extremum. Hint: show that there is no integral F for which the variation is of the form

$$\delta F = \int [(\boldsymbol{v} \cdot \boldsymbol{\nabla})\boldsymbol{v} - \nu \boldsymbol{\nabla}^2 \boldsymbol{v} + \boldsymbol{\nabla} p/\rho_0] \cdot \delta \boldsymbol{v} \, dV \tag{19-28}$$

(which vanishes for all $\boldsymbol{v}$ satisfying (18-4)).

19.2 Show that the Poisson equation

$$\boldsymbol{\nabla}^2 q = s \tag{19-29}$$

is the minimum of the quadratic 'energy' function

$$\mathcal{E} = \int_V \left(\frac{1}{2} (\boldsymbol{\nabla} q(\boldsymbol{x}))^2 + q(\boldsymbol{x}) q(\boldsymbol{x}) \right) dV \ , \tag{19-30}$$

under suitable boundary conditions. Use this result to devise a gradient descent algorithm towards the minimum. What is the discrete form of the 'energy'?

19.3 Indicate in fig. 19.1 which staggered grids naturally carry the various stress components, σ_{xx}, σ_{yy}, and σ_{xy}.

19.4 Verify that the various averages in F_x in terms of the grid arrays become

$$\begin{aligned}
\left\langle \widehat{\nabla}_x v_x \right\rangle [i_x, i_y] &= \frac{v_x[i_x+1, i_y] - v_x[i_x-1, y]}{2\Delta x} \\
\langle v_y \rangle [i_x, i_y] &= \frac{v_y[i_x, i_y] + v_y[i_x+1, i_y] + v_y[i_x, i_y-1] + v_y[i_x+1, i_y-1]}{4} \\
\left\langle \widehat{\nabla}_y v_x \right\rangle [i_x, i_y] &= \frac{v_x[i_x, i_y+1] - v_x[i_x, y-1]}{2\Delta y}
\end{aligned}$$

And in F_y

$$\begin{aligned}
\langle v_x \rangle [i_x, i_y] &= \frac{v_x[i_x, i_y] + v_x[i_x-1, i_y] + v_x[i_x, i_y+1] + v_x[i_x-1, i_y+1]}{4} \\
\left\langle \widehat{\nabla}_x v_y \right\rangle [i_x, i_y] &= \frac{v_y[i_x+1, i_y] - v_y[i_x-1, y]}{2\Delta x} \\
\left\langle \widehat{\nabla}_y v_y \right\rangle [i_x, i_y] &= \frac{v_y[i_x, i_y+1] - v_y[i_x, y-1]}{2\Delta y}
\end{aligned}$$

Copyright © 1998–2002, Benny Lautrup